New perspective of fracture mechanics inspired by gap test with crack-parallel compression

Hoang Nguyen[a], Madura Pathirage[a], Masoud Rezaei[b], Mohsen Issa[b], Gianluca Cusatis[a], and Zdeněk P. Bažant[a,1]

[a]Department of Civil and Environmental Engineering, Northwestern University, Evanston, IL 60208; and [b]Department of Civil and Materials Engineeirng, University of Illinois at Chicago, Chicago, IL 60607

Contributed by Zdeněk P. Bažant, April 22, 2020 (sent for review March 30, 2020; reviewed by Huajian Gao and Ares J. Rosakis)

The line crack models, including linear elastic fracture mechanics (LEFM), cohesive crack model (CCM), and extended finite element method (XFEM), rest on the century-old hypothesis of constancy of materials' fracture energy. However, the type of fracture test presented here, named the gap test, reveals that, in concrete and probably all quasibrittle materials, including coarse-grained ceramics, rocks, stiff foams, fiber composites, wood, and sea ice, the effective mode I fracture energy depends strongly on the crack-parallel normal stress, in-plane or out-of-plane. This stress can double the fracture energy or reduce it to zero. Why hasn't this been detected earlier? Because the crack-parallel stress in all standard fracture specimens is negligible, and is, anyway, unaccountable by line crack models. To simulate this phenomenon by finite elements (FE), the fracture process zone must have a finite width, and must be characterized by a realistic tensorial softening damage model whose vectorial constitutive law captures oriented mesoscale frictional slip, microcrack opening, and splitting with microbuckling. This is best accomplished by the FE crack band model which, when coupled with microplane model M7, fits the test results satisfactorily. The lattice discrete particle model also works. However, the scalar stress–displacement softening law of CCM and tensorial models with a single-parameter damage law are inadequate. The experiment is proposed as a standard. It represents a simple modification of the three-point-bend test in which both the bending and crack-parallel compression are statically determinate. Finally, a perspective of various far-reaching consequences and limitations of CCM, LEFM, and XFEM is discussed.

fracture energy | cohesive crack model | finite element crack band model | softening damage | quasibrittle materials

The linear elastic fracture mechanics (LEFM), originated by Griffith in 1921 (1), and the cohesive crack model (CCM), introduced by Barenblatt in 1959 (2), are line crack models that do not include the crack-parallel strain ϵ_{xx} among the basic thermodynamic variables, and thus cannot take the crack-parallel normal stress σ_{xx} properly into account. This is because a zero-width fracture process zone (FPZ) is considered. Thus the crack-parallel normal stress σ_{xx} can enter the LEFM or CCM only as a parameter of the fracture energy. Then, however, one cannot distinguish different histories of crack-parallel stress, and their effects on the relative displacements of crack faces and on the stress–strain tensors in the FPZ. Therefore, a FPZ of finite width must be modeled, reflecting its mesoscale physical behavior. The possibilities are a tensorial damage softening constitutive law coupled with crack band model (CBM) (3), the nonlocal models (4), or the lattice discrete particle model (LDPM) (5–7).

The softening law must capture the difference between 1) the total fracture energy, G_F, which represents the area under the traction–separation curve in CCM, and 2) the initial fracture energy, G_f, which is the area under the initial tangent of the traction–separation curve and is the key parameter for predicting the load capacity of concrete specimens and structures (8, 9) (see Fig. 1*F*). Both CCM and LDPM can capture this difference. Typically, $G_F/G_f \approx 2$ to 6 for concretes. G_f is what governs the maximum loads of most structures, while G_F usually matters only for energy adsorption, for example, under impact.

High crack-parallel stresses are important for all quasibrittle materials such as concrete, shale, coal and various rocks, stiff soils, tough or toughened ceramics, bone and many biomaterials, fiber composites, sea ice, printed solids, rigid foams, and wood, because these materials exhibit similar mesoscale mechanisms. All brittle materials become quasibrittle on micrometer or nanometer scales. The importance of considering a finite width of FPZ is supported by futile experience with the cohesive crack modeling of size effect in shear failure of reinforced concrete (RC) beams and slabs, which has been a formidable problem for decades. A crack of nearly mode I type, driven by shear force, propagates in a stable manner through about 80% of the cross-section depth, and the failure eventually occurs because of crack-parallel compression at the crack front (see Fig. 2 *C* and *D*). Another example is the gross overestimation of the forces exerted by sea ice on the legs of oil platforms. Neither LEFM nor CCM could ever fit the data, but the CBM (with M7) (8, 10–13) and the LDPM (14, 15) could. This experience is what partly inspired this study.

The micromechanism of compression damage and fracture in these materials consists of lateral expansion due to splitting and slip along inclined microcracks or along weak interfaces between inhomogeneities. Metals, on the micrometer scale, exhibit progressive strain softening [due to void growth or grain boundary mismatch (16), or to hydrogen embrittlement (17)], and so σ_{xx} must have an effect at that scale, too. Similarly, such stresses play a nonnegligible role in hydraulic fracturing of shale at 3-km depth, as they are nearly equal to the uniaxial compression

Significance

Fracture mechanics has long been an essential tool for ensuring safety, efficiency, and durability in the mechanical, aerospace, nuclear, naval, petroleum, and other industries. Recently, with the adoption of fracture-based size effect law for design code of American Concrete Institute (ACI-318), fracture mechanics has also become the basis of designing concrete structures against quasibrittle failures. The present experimental discovery will improve the fracture predictions for concrete, rock (including shale), fiber composites, tough ceramics, sea ice, wood, and other quasibrittle materials.

Author contributions: H.N. and Z.P.B. designed research; H.N. and M.P. produced test specimens; H.N., M.P., M.R., and M.I. performed experiments; H.N., M.P., and M.R. analyzed test results; H.N., M.P., M.R., M.I., G.C., and Z.P.B. discussed the results; and H.N. and Z.P.B. wrote the paper.

Reviewers: H.G., Nanyang Technological University; and A.J.R., California Institute of Technology.

The authors declare no competing interest.

Data deposition: The data from the experiments and simulations can be found at the author's Github repository: github.com/htn403/PNAS_MS-2020-05646.

[1]To whom correspondence may be addressed. Email: z-bazant@northwestern.edu.

First published June 9, 2020.

strength, σ_c (18). High σ_{xx} also arises in composite laminates in aircraft and automobile crush cans, sea ice floes pushing against oil platform, pavement cracks under wheel loads, etc.

Relevant Previous Studies

The effect of crack-parallel stresses in quasibrittle materials has been widely ignored. The reason, obviously, is that, for line crack models (LEFM, CCM), a line crack cut along x direction in a uniform field of σ_{xx} causes, of course, no stress change. This might be why all of the standard notched fracture test specimens—three-point-bend (3PB), single-edge-notched tension, circumferentially notched tension, diametral compression, compact tension, double cantilever, edge-notched eccentric compression, etc.—have near-zero σ_{xx}. The wedge-splitting specimen might seem to be an exception, but the $|\sigma_{xx}|$ is insignificant compared with the uniaxial compression strength, f_c, and is nonnegligible only at some distance from the FPZ.

Another reason for experiments with negligible σ_{xx} might have been to shun the complexity of applying additional loads, which leads to ambiguity. In structural engineering laboratories, tests with multiple loads are, of course, commonplace, but they require the use of multiple hydraulic jacks, which introduce undesirable self-weight loads and lead to a statically indeterminate support system in which stress evaluation requires a damage constitutive law which may not be well understood.

Hydraulic jacks causing crack-parallel compression were used in 1995 by Tschegg et al. (19) in an elaborate modification of the wedge-splitting test. The results confirmed the hint from the 1987 microplane model that crack-parallel compression should matter. However, the evaluation was aimed at G_F rather than G_f, and thus was compromised by unknown shape, at that time, of the complete softening law (as in Fig. 1*F*), and suffered from the complexity of the stress field due to the weight of heavy clamping frames, and to friction under the jacks. Bigger problems were the lack of tests at different sizes, without which the work-of-fracture method is now known to give ambiguous results (20), due to the FPZ size variation near notch tip and near opposite boundary.

The effect of σ_{xx}, called the T-stress, was also considered in fracture of plastic metals (21–24). Triaxiality of stress state in a tip-surrounding annulus, with extra parameter Q as the relative difference between stress fields when T is or is not zero, led to a monotonic increase of the critical J-integral value based on the Hutchinson–Rice–Rosengren (25, 26) field. These results, however, are not transplantable to quasibrittle materials, in which the physics is different (Fig. 2*E*) and the σ_{xx} effect can be nonmonotonic. Moreover, the impact of biaxial in-and-out-of-plane stresses seems not to have been studied for metals. The T-stress effect was also analyzed in ref. 27, but for a different purpose—curved deflection of the LEFM crack path.

In numerical analysis, the simplest and the most widely used method for quasibrittle fracture of concrete and geomaterials is the CBM (3). It requires a realistic tensorial constitutive

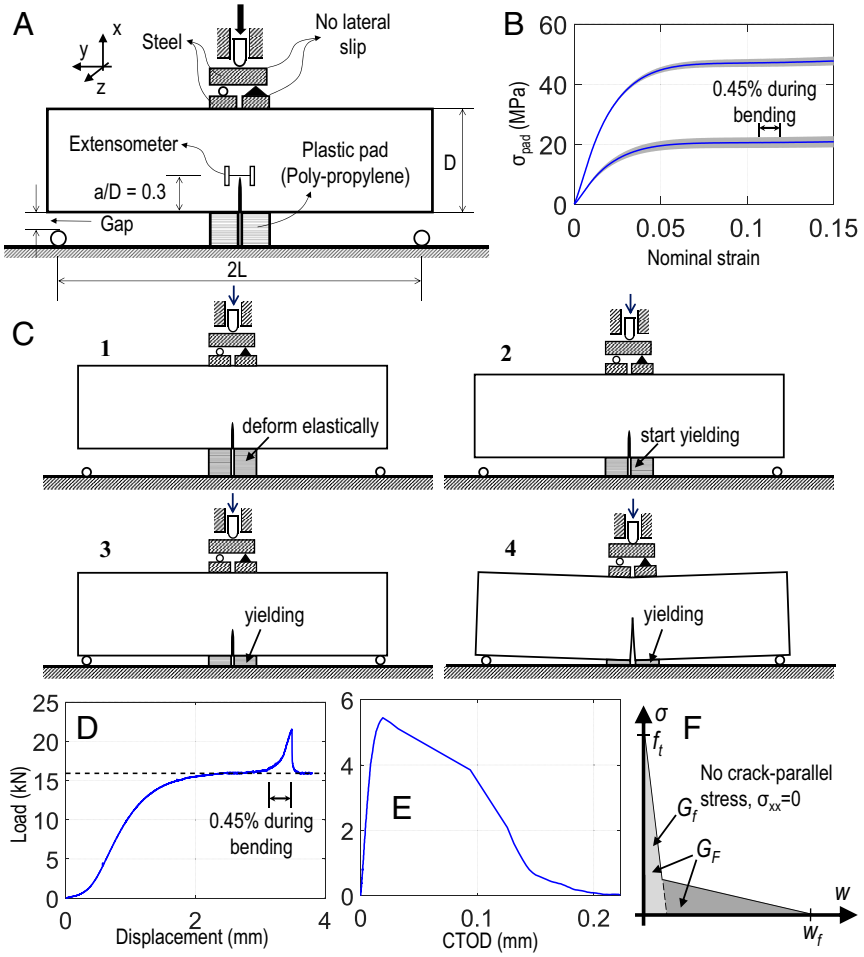

Fig. 1. (*A*) Experimental setup of the gap test. (*B*) Stress–strain behavior of plastic pad corresponding to two values of tested σ_{xx}. (*C*) Experimental procedure. (*D*) Typical load–machine displacement behavior. (*E*) Extracted load–CTOD. (*F*) Traction–separation curve without crack-parallel stress.

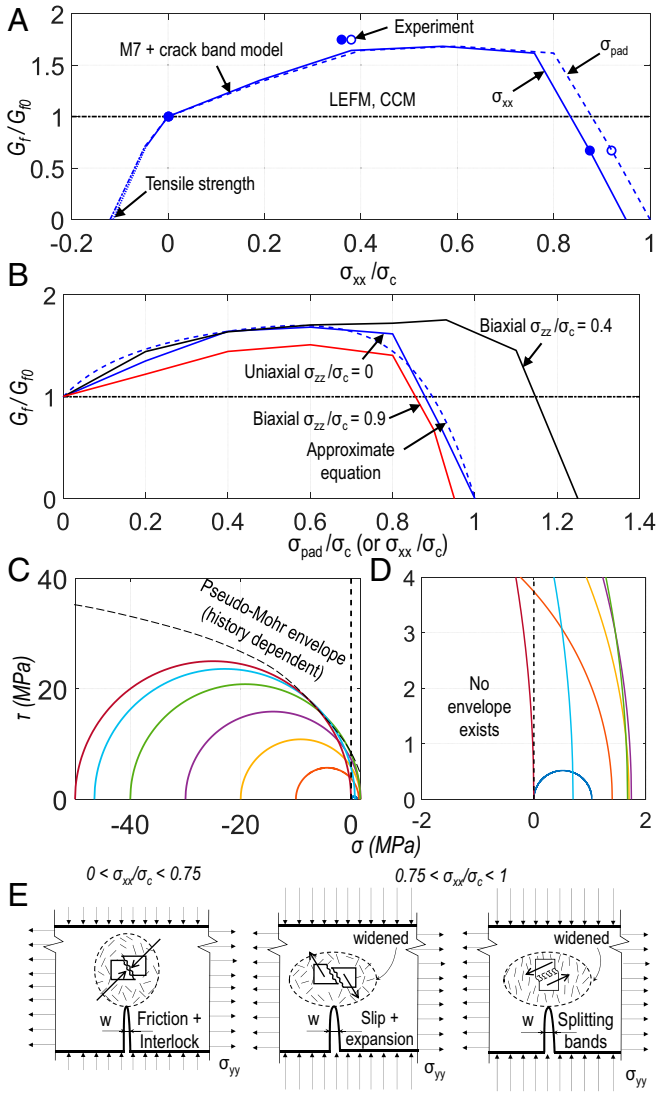

Fig. 2. (*A*) G_f as a function of σ_{pad} (dashed curve) and of σ_{xx} (solid curve). (*B*) G_f as a function of σ_{xx} subject to different values of antiplane stress σ_{zz} ($a = 1.038$, $b = 0.245$, $c = 7.441$ in Eq. **1**). (*C*) Mohr circles corresponding to the M7 results in *A*, with σ_{yy} as nominal strength at peak load. (*D*) A zoom into the region of small σ_{xx}. (*E*) Proposed mechanisms for increase and decrease of G_f.

law for softening damage (28, 29), so as to capture implicitly the mechanisms in Fig. 2*E*. An alternative is an explicit mesoscale particle model, for example, refs. 6 and 7. The microplane model for concrete, particularly its latest version, M7 (28, 29), employed here, has been shown to reproduce the dilatant slip and splitting closely. However, the CCM with a unique traction–separation law for a line crack, the LEFM used in XFEM (30), and the tensorial damage band models governed by a single parameter (31–33) cannot capture the σ_{xx} effect.

Fracture Test with Crack-Parallel Compression

To demonstrate and measure the σ_{xx} effect, we develop a surprisingly simple test of notched beams, named the gap test, with four crucial features: 1) plastic support pads with near-perfect plastic yielding introduce, at first, notch-parallel compression σ_{xx}; 2) rigid end supports are installed with gaps and engage only after constant σ_{xx} begins to act, which 3) delivers a support system that switches from one statically determinate configuration to another, thus allowing unambiguous interpretation; and 4) the test configuration is, at the same time, suitable for the size effect method which is needed for evaluating the fracture energy G_f and characteristic FPZ size c_f unambiguously. In this experiment, depicted in Fig. 1*A* (as developed at Northwestern University), a notched 3PB concrete beam is placed on two kinds of sequentially engaged statically determinate supports: 1) two symmetric pairs of initially contacting polypropylene pads, one pair immediately adjacent to the sides of the notch, and 2) a pair of stiff cylindrical supports installed with initial small gaps at beam ends.

The pads initially deform elastically and, subsequently, exhibit a long, almost horizontal, yield plateau, shown in Fig. 1*B*. The magnitude of the maximum yield force, for a given pad area in contact with the specimen, can be controlled by piercing the pad with holes, which allows application of different levels of stress parallel to the notch. The center-span load is applied through a pair of steel plates located symmetrically to the plastic pads.

Until the support gaps at the ends close, the only loading is by two compression forces along the notch plane, with only negligible bending due to the self-weight. The pair of steel plates at the top is mildly restrained against rotation, to ensure stability. Shortly after the pads begin to yield, the stiff end supports engage in contact and produce a bending moment which increases until the maximum load is reached, while, thanks to plastic yielding of the pads, the crack-parallel compression force remains constant. Thus the bending action, which is what opens the crack, is statically determinate.

The compressive stress in the FPZ, σ_{xx}, which is what matters to the material property, is proportional to, but only slightly smaller than, the compressive stress under the pads, σ_{pad}. The reduction ratio, $r_c = \sigma_{xx}/\sigma_{pad}$, obtained by crack band finite element (FE) analysis, is about 0.96, although nonlinear analysis would give a slight (and virtually negligible) variation of r_c with P and structure size. To prevent notch mouth corners from shearing off under the pad force, short and thin laminate sheets are glued at the bottom adjacent to the notch. Their effect on the stress intensity factor is negligible. The crack-tip opening displacement δ_{CTOD} is measured by an extensometer (Fig. 1*A*). After reaching P_{max}, the curve of load P versus load-point displacement drops to the yield load value (Fig. 1*D*), and the beam then fractures completely.

Since the plasticized polymer in the pads is incompressible, it gets squeezed laterally from the pads. The tangential stiffness of the rectangular pads of width $l \ll$ length L can be shown to be $H = L(\mu)(l/h)^3$, where h is thickness of the plasticized polymer layer, l is its length (in two dimensions), and μ is tangential shear modulus of the plasticized polymer (with no holes), which is very small but inevitably nonzero (or else the squeezed polymer would flow out like a fluid). H needs to be also very small, and so l/h should be minimized in pad design.

What made the G_f measurement possible was to test specimens of various sizes and apply the size effect method (34), which is the most robust approach to measure the initial fracture energy G_f (and c_f). It has been adopted as an international standard recommendation (35) and endorsed by ACI-446 (36). It is based on the size effect law for quasibrittle fracture (10, 34, 37, 38). It has become the most widely used method for testing G_f of concrete and geomaterials. One advantage is that it necessitates measuring only P_{max} (no postpeak), although for at least three sufficiently different specimen sizes (8, 34, 39). As another advantage, the identification of G_f along with the characteristic FPZ size c_f is reducible to linear regression. Importantly, the derivation of this method (8, 34) is not affected by the crack-parallel stress, neither in-plane σ_{xx} nor out-of-plane σ_{zz}.

The experiments used normal concrete with mean cylindrical compression strength f_c = 40.5 MPa, maximum aggregate size 18 mm, span-to-depth ratio $2L/D$ = 3.75, and notch depth ratio a/D = 0.3. Beams of three depths D = 101.6 mm (4 in), 203.2 mm (8 in), and 406.4 mm (16 in) were scaled geometrically. The specimen thickness was 101.6 mm for all sizes. A typical measured curve of load P vs. load–point displacement u and the curve of P versus δ_{CTOD} is shown for D = 101.6 mm in Fig. 1 *D* and *E*.

The three data points (empty circles) in Fig. 2*A*, based on regression of data from $3 \times 9 = 27$ gap tests, are the evaluated effective values of fracture energy G_f as a function of three levels of compression stress σ_{pad} applied at the yielding pads. Obviously, G_f is not constant but strongly depends on σ_{pad}. This suffices to raise doubts about the applicability of both the LEFM and the CCM, both of which require constancy of G_f. To get the effective G_f as a material property, the data are scaled by r_c to the σ_{xx} values at notch tip—the solid circle points in Fig. 2*A*.

Alternatively, according to the classical work-of-fracture method (40–42), one could estimate the total fracture energy, G_F, via the area between the whole up-and-down curve and the horizontal yield line in Fig. 1*A*. However, this method requires stabilizing the postpeak softening and is rather ambiguous if the correct shape of the cohesive law, Fig. 1*F*, is not known a priori (20). To avoid ambiguity of G_F, the work-of-fracture test must be conducted at several sufficiently different specimen sizes (20). Hence, to measure how G_F depends on σ_{xx}, the present test would have to be extended into the whole postpeak for all of the sizes D.

Fitting and Evaluation of Test Results Using Microplane Model M7

The simplest and most widely used FE method to suppress spurious mesh sensitivity caused by localization instability of strain-softening damage is the CBM (3, 8, 43). In a quasibrittle material (i.e., a heterogenous material with brittle constituents and inhomogeneities or grains not negligible compared to structure size), the crack, blunted at front by a long and wide FPZ, is modeled by a band of FE of width h representing a material property; $h = G_{f\,0}/A$, where A is the area under the curve of stress versus relative displacement and $G_{f\,0}$ is the G_f value for $\sigma_{xx} = 0$. The precise h value is not too important, but the same h must be used for different structure sizes D. Alternatively, if the postpeak of the stress–separation curve is scaled so that Ah would give the same G_f, then h can be changed, with some loss in accuracy. Here, h is kept the same for all D.

The microplane model M7 (28, 29) presented here is the latest version of microplane models whose development began in 1983. In this model, the damage constitutive law is defined in terms of stress and strain vectors acting on mesoscale planes, called the microplanes, which sample, discretely, all spatial orientations according to an optimal Gaussian numerical integration formula for a spherical surface. The use of vectors permits a direct physical modeling of oriented cracking, splitting, and frictional slip, which is crucial for describing the complex stress state in the FPZ. For softening damage, the strain vector is projected from the continuum strain tensor, upon which the stress vectors on all of the microplanes are used in the variational principle of virtual work to obtain the stress tensor. M7 has been shown to be give good predictions in complex fracture problems and is featured in various softwares. Here M7 is implemented as user-defined material into the commercial software ABAQUS. Six-node wedge elements are used.

The FE program with CBM and M7 was calibrated so as to give the correct values of uniaxial compression strength and G_f at $\sigma_{xx} = 0$, which is the first data point in Fig. 2*A*. This calibration sufficed for the FE program with M7 to match closely the tensile material tests. The same FE program was then used to predict the G_f for many applied pressures σ_{pad}, which led to the dashed curve in Fig. 2*A*, plotted in dimensionless coordinate $\xi_{pad} = \sigma_{pad}/\sigma_c$. Note that this curve matches satisfactorily (within inevitable experimental scatter) the empty circles showing the measured Gf.

However, the plot of G_f vs. ξ_{pad} does not represent a material property. What does is the plot of G_f vs. $\xi = \sigma_{xx}/\sigma_c = r_c\sigma_{pad}/\sigma_{xx}$, corresponding to σ_{xx} values at notch tip. The measured data for G_f are shifted by the same ratio r_c and are shown by the solid circle points. For comparison, ratio r_c calculated by a linearly elastic FE program with a stress-free crack band is $r_{c,el}$ = 0.942 for the medium-size specimens, 0.981 for the smallest, and 0.925 for the largest; 0.942 is so close to 0.962 that $r_{c,el}$ should suffice, in practice.

The agreement of the predicted curve with the three data points in Fig. 2*A* is satisfactory. This observation lends enhanced credence to the test.

Intuitive Explanation of G_f Variation by a Microstructural Mechanism

Can the observed dependence of G_f on crack-parallel stress ratio ξ be plausibly explained physically? It can, by the mechanisms schematized in Fig. 2*E* (44).

1) To explain the initial rising part of the curve in Fig. 2*A*, note that a major part of the mode I fracture energy of concrete is dissipated by frictional slip on microcracks inclined with respect to the directions of macrocrack propagation (45) and by grain interlock enhanced by surface roughness, rather than by opening of tensile microcracks. A pressure on the inclined microcrack as a projection of crack-parallel stress will obviously increase the resistance to slip. This feature explains why, in concrete, the curve of effective G_f versus ξ is initially rising.
2) To explain the second, descending, part of the curve in Fig. 2*A*, note that a higher crack-parallel compression overcomes friction and causes the inclined microcrack to slip, which, in turn, causes lateral expansion with axial splitting cracks (Fig. 2*E*). Another possible mechanism is the formation of inclined bands of axial splitting cracks (44), which also leads to slip with lateral expansions (Fig. 2*E*) of width s. Both must cause the FPZ to widen.

Can Mohr failure envelope be used to predict incipient failure? The Mohr circles for the subsequent stress states in FPZ are plotted in Fig. 2 *C* and *D* (σ is hydrostatic stress, τ is maximum shear stress). The first slip mechanism, frictional resistance with no damage, seems to follow a curved Mohr failure envelope with strength expanding at moderate increase of hydrostatic pressure (Fig. 2*C*). However, when the second mechanism with expansive damage takes over, the Mohr envelope concept breaks down. This is blatantly demonstrated by zooming, in Fig. 2*D*, on the critical region of small σ and τ. Obviously, no envelope exists. This is not surprising, since the plasticity-type failure criteria based on tensor invariants are inherently incapable of capturing the concentration of slip into planes of distinct orientations, which represent the reality.

Since the first mechanism is not typical of fiber composites, it is suspected that, unlike Fig. 2 *A* and *B*, their $G_f(\xi)$-curve would normally be descending monotonically. This would mean that crack-parallel compression is more dangerous than in concrete.

Proposal for a Standard Fracture Test

It now becomes clear that, for quasibrittle materials, the currently standardized fracture tests provide insufficient information. Since, in reinforced concrete, geomechanics, or structural composites, cracks with significant crack-parallel compression or

tension often occur in finite element analysis, societies such as ASTM (American Society for Testing and Materials) or RILEM (International Union of Laboratories and Experts in Construction Materials, Systems and Structures, Paris) should consider introducing a standard test. The present test appears to be a good candidate.

Vision of Fracture Mechanics Future

Although the present experiments demonstrate the importance of crack-parallel stress, they are too limited to justify immediate sweeping changes in fracture mechanics practice. Nevertheless, in the light of these experiments, it is already obvious that an extensive program of experiments, theoretical modeling, and numerical simulations is called for. Such a program will, of course, require time, significant funding, and teams of investigators.

So, at this centennial anniversary of Griffith's founding of fracture mechanics (1921), we content ourselves merely with offering a vision of the future.

1) It will be necessary to determine all of the consequences of crack-parallel compression or tension, in-plane, anti-plane and combined, for the apparent fracture energy in mode I, and doubtless also modes II and III, and mixed mode—for concretes of diverse types, shale and various other rocks, fiber composites, toughened ceramics, rigid foams, bone, printed solids, sea ice, and many other quasibrittle materials. Anisotropic materials such as shale or fiber composites will surely show more diversity. Because of the well-known weakness in compression of fiber composites, especially the unidirectional ones, and the absence of friction and interlocking, a strong monotonic decrease of effective G_f with crack-parallel compression is expected. The histories of σ_{xx} and σ_{zz} (and probably also in-plane shear stress) will doubtless make a difference, too.
2) Major implications can be expected for the hydraulic fracturing of shale, typically conducted at 3-km depth, at which the crack-parallel compression along a vertical crack, due to tectonic stress and overburden, is near the uniaxial strength limit.
3) The fracture energy of geological faults causing earthquakes is another tantalizing problem. Very narrow though the fault slip zone is, the FPZ at the front of propagating fault slip might nevertheless be wide enough for the huge tectonic stress parallel to fault to have an effect.
4) In view of the mechanism sketched in Fig. 2*E*, it is expected that, in coarse ceramics, concrete, and other quasibrittle materials, the crack-parallel compression would accelerate cyclic and static fatigue crack propagation, increasing the prefactor of Paris law and Charles–Evans law, and perhaps altering the exponent. The size dependence of these laws (8, 10, 46, 47), particularly the transition size D_0, might also get modified.
5) Fiber reinforcement of concrete tends to mitigate the compression splitting, which is explained by inhibition of the microscale splitting as in Fig. 2*E*. Fibers are thus expected to prolong the initial rise of the G_f curves in Fig. 2*A* and to postpone their final descent.
6) While the crack-parallel stress has a very different, and already known, effect in plastic-hardening metals, the micrometer scale might be an exception (48), because quasibrittle behavior such as gradual postpeak softening with size effect has been observed on thin metallic films. This could matter for microelectromechanical system substrates and may be worth investigation.
7) As it now appears, neither the CCM- nor the LEFM-based models should be used in general purpose FE software for quasibrittle structures. This includes XFEM (30), based on LEFM, and also damage band models based on a one-parameter tensorial damage law (31, 32, 49) which cannot fit the triaxial material tests of various types (28) obtained on specimens of roughly the same size as the FPZ [the so-called "peridynamics" needs no comment (50)]. These models are usable only if it is known a priori that the crack-parallel normal stresses, both in-plane and out-of-plane (and in-plane shear), are negligible. To capture the effects of these stresses, fracture must be modeled as a band with a realistic tensorial softening damage model, preferably based on vectorial constitutive stress–strain relations that can capture orientation effects, as in microplane or mesomechanical models such as LDPM.
8) The need for tensorial characterizations of FPZ was suggested in a recent approach (e.g., ref. 51) in which a band with softening constitutive damage law is shrunken into a line, so as to enrich the stress–displacement relation of a cohesive line crack by an embedded subscale tensorial band. A step in the right direction though this was, the formulation was not shown capable of describing the crack-parallel stress effects and reproducing the effects of triaxial stress history and of nonproportional evolution of stress and strain tensor components in the FPZ. Also, after shrinking the damage band of finite width into a line crack, the minimum possible spacing of parallel cracks does not get enforced.
9) The importance of considering a tensorial FPZ of finite width, as in CBM, or material heterogeneity, as in LDPM, is blatantly demonstrated by 1) the futile experience with the LEFM and CCM of size effect in shear failure of RC beams and slabs or 2) gross overestimation of the measured force exerted on the legs of oil platforms by a moving ice plate.
10) The Mohr failure envelope has been widely used to assess incipient fracture of shale, and slip in geophysics. However, due to high σ_{xx}, this is unrealistic.
11) The curve in Fig. 2 *A* and *B* can be closely approximated by

$$G_f/G_{f0} = 1 + a/(1 + b/\xi) - (1 + a + b)/(1 + b)\xi^c, \qquad [1]$$

where f_c is compression strength. Constants a, b, c are different for different materials, structure sizes, load histories, σ_{zz}/σ_{xx} ratios, etc. Having such formulas for various situations, the existing software for cohesive cracks, LEFM, XFEM, or phase-field model could be adapted to variable fracture energy, as a crude approximation. But there seems no good general way to avoid crack band or mesoscale simulations.

Afterthought. Many hot research subjects become closed in a few decades. But, like turbulence, fracture mechanics is different. This formidable subject has been researched for a century, and probably will be for another century.

Data Availability. The data from the experiments and simulations can be found at the author's Github repository: github.com/htn403/PNAS_MS-2020-05646.

ACKNOWLEDGMENTS. We acknowledge partial preliminary funding under NSF Grant CMMI-1439960 to Northwestern University, and valuable comments by Jialing Le and Marco Salviato.

1. A. Griffith, The phenomena of rupture and flow in solid, *Philos. Trans. Roy. Soc. London Ser. A* **221**, 163–193 (1921).
2. G. I. Barenblatt, Equilibrium cracks formed on a brittle fracture. *Dokl. Ak. N.* **127**, 47–50 (1959).
3. Z. P. Bažant, B. H. Oh, Crack band theory for fracture of concrete. *Mat. Constr.* **16**, 155–177 (1983).
4. Z. P. Bažant, M. Jirásek, Nonlocal integral formulations of plasticity and damage: Survey of progress. *J. Eng. Mech.* **128**, 1119–1149 (2002).

5. G. Cusatis, Z. P. Bažant, L. Cedolin, Confinement-shear lattice model for concrete damage in tension and compression: I. Theory. *J. Eng. Mech.* **129**, 1439–1448 (2003).
6. G. Cusatis, D. Pelessone, A. Mencarelli, Lattice discrete particle model (LDPM) for failure behavior of concrete. I. Theory. *Cem. Concr. Compos.* **33**, 881–890 (2011).
7. G. Cusatis, A. Mencarelli, D. Pelessone, J. Baylot, Lattice discrete particle model (LDPM) for failure behavior of concrete. ii: Calibration and validation. *Cem. Concr. Compos.* **33**, 891–905 (2011).
8. Z. P. Bažant, J. Planas, *Fracture and Size Effect in Concrete and Other Quasibrittle Materials* (CRC Press, Boca Raton, FL, 1998).
9. G. Cusatis, E. A. Schauffert, Cohesive crack analysis of size effect. *Eng. Fract. Mech.* **76**, 2163–2173 (2009).
10. Z. P. Bažant, *Scaling of Structural Strength* (CRC Press, Boca Raton, FL, 2002).
11. Z. P. Bažant, Q. Yu, Designing against size effect on shear strength of reinforced concrete beams without stirrups: II. Verification and calibration. *J. Struct. Eng.* **131**, 1886–1897 (2005).
12. Q. Yu *et al.*, Comparison of main models for size effect on shear strength of reinforced and prestressed concrete beams. *Struct. Concr.* **17**, 778–789 (2016).
13. A. Dönmez, Z. P. Bažant, Size effect on punching strength of reinforced concrete slabs with and without shear reinforcement. *ACI Struct. J.* **114**, 875–866 (2017).
14. M. Alnaggar, D. Pelessone, G. Cusatis, Lattice discrete particle modeling of reinforced concrete flexural behavior. *J. Struct. Eng.* **145**, 04018231 (2019).
15. E. Lale, R. Rezakhani, M. Alnaggar, G. Cusatis, Homogenization coarse graining (hcg) of the lattice discrete particle model (LDPM) for the analysis of reinforced concrete structures. *Eng. Fract. Mech.* **197**, 259–277 (2018).
16. Z. P. Bažant, Z. Guo, H. D. Espinosa, Y. Zhu, B. Peng, Epitaxially influenced boundary layer model for size effect in thin metallic films. *J. Appl. Phys.* **97**, 073506 (2005).
17. Y. Deng, A. Barnoush, Hydrogen embrittlement revealed via novel in situ fracture experiments using notched micro-cantilever specimens. *Acta Mater.* **142**, 236–247 (2018).
18. S. Rahimi-Aghdam *et al.*, Branching of hydraulic cracks enabling permeability of gas or oil shale with closed natural fractures. *Proc. Natl. Acad. Sci. U.S.A.* **116**, 1532–1537 (2019).
19. E. K. Tschegg, M. Elser, S. E. Stanzl-Tschegg, Biaxial fracture tests on concrete—development and experience. *Cem. Concr. Compos.* **17**, 57–75 (1995).
20. C. G. Hoover, Z. P. Bažant, Cohesive crack, size effect, crack band and work-of-fracture models compared to comprehensive concrete fracture tests. *Int. J. Fract.* **187**, 133–143 (2014).
21. N. P. O'Dowd, C. F. Shih, Family of crack-tip fields characterized by a triaxiality parameter—I. Structure of fields. *J. Mech. Phys. Solids* **39**, 989–1015 (1991).
22. N. P. O'Dowd, C. F. Shih, Family of crack-tip fields characterized by a triaxiality parameter—II. Fracture applications. *J. Mech. Phys. Solids* **40**, 939–963 (1992).
23. C. Betegón, J. W. Hancock, Two-parameter characterization of elastic-plastic crack-tip fields. *J. Appl. Mech.* **58**, 104–110 (1991).
24. V. Tvergaard, J. W. Hutchinson, The relation between crack growth resistance and fracture process parameters in elastic-plastic solids. *J. Mech. Phys. Solids* **40**, 1377–1397 (1992).
25. J. W. Hutchinson, Singular behaviour at the end of a tensile crack in a hardening material. *J. Mech. Phys. Solids* **16**, 13–31 (1968).
26. J. R. Rice, G. F. Rosengren, Plane strain deformation near a crack tip in a power-law hardening material. *J. Mech. Phys. Solids* **16**, 1–12 (1968).
27. B. Cotterell, J. R. Rice, Slightly curved or kinked cracks. *Int. J. Fract.* **16**, 155–169 (1980).
28. F. C. Caner, Z. P. Bažant, Microplane model M7 for plain concrete. I: Formulation. *J. Eng. Mech.* **139**, 1714–1723 (2013).
29. F. C. Caner, Z. P. Bažant, Microplane model M7 for plain concrete. II: Calibration and verification. *J. Eng. Mech.* **139**, 1724–1735 (2013).
30. N. Moës, J. Dolbow, T. Belytschko, A finite element method for crack growth without remeshing. *Int. J. Numer. Methods Eng.* **46**, 131–150 (1999).
31. B. Bourdin, G. A. Francfort, J.-J. Marigo, The variational approach to fracture. *J. Elast.* **91**, 5–148 (2008).
32. M. J. Borden, C. V. Verhoosel, M. A. Scott, T. J. R. Hughes, C. M. Landis, A phase-field description of dynamic brittle fracture. *Comput. Meth. Appl. Mech. Engrg.* **217**, 77–95 (2012).
33. J. Vignollet, S. May, R. De Borst, C. V. Verhoosel, Phase-field models for brittle and cohesive fracture. *Meccanica* **49**, 2587–2601 (2014).
34. Z. P. Bažant, M. T. Kazemi, Size effect in fracture of ceramics and its use to determine fracture energy and effective process zone length. *J. Am. Ceram. Soc.* **73**, 1841–1853 (1990).
35. RILEM Recommendation TC89-FMT, Size-effect method for determining fracture energy and process zone size of concrete. *Mater. Struct.* **23**, 461–465 (1990).
36. ACI Committee 446, Fracture mechanics of concrete: Concepts, models and determination of material properties (Special publication IR-91, American Concrete Institute, 1992).
37. Z. P. Bažant, Size effect in blunt fracture: Concrete, rock, metal. *J. Eng. Mech.* **110**, 518–535 (1984).
38. Z. P. Bažant, Scaling of quasibrittle fracture: Asymptotic analysis. *Int. J. Fract.* **83**, 19 (1997).
39. Z. P. Bažant, L. Jia-Liang, *Probabilistic Mechanics of Quasibrittle Structures: Strength, Lifetime, and Size Effect* (Cambridge University Press, 2017).
40. J. Nakayama, Direct measurement of fracture energies of brittle heterogeneous materials. *J. Am. Ceram. Soc.* **48**, 583–587 (1965).
41. H. G. Tattersall, G. Tappin, The work of fracture and its measurement in metals, ceramics and other materials. *J. Mater. Sci.* **1**, 296–301 (1966).
42. A. Hillerborg, M. Modéer, P.-E. Petersson, Analysis of crack formation and crack growth in concrete by means of fracture mechanics and finite elements. *Cem. Concr. Res.* **6**, 773–781 (1976).
43. J. Červenka, Z. P. Bažant, M. Wierer, Equivalent localization element for crack band approach to mesh-sensitivity in microplane model. *Int. J. Numer. Meth. in Eng.* **62**, 700– 726 (2005).
44. Z. P. Bažant, Y. Xiang, Size effect in compression fracture: Splitting crack band propagation. *J. Eng. Mech.* **123**, 162–172 (1997).
45. Z. P. Bažant, W. F. Schell, Fatigue fracture of high-strength concrete and size effect. *ACI Mater. J.* **90**, 472–472 (1993).
46. Z. P. Bažant, K. Xu, Size effect in fatigue fracture of concrete. *ACI Mater. J.* **88**, 390–399 (1991).
47. K. Kirane, Z. P. Bažant, Microplane damage model for fatigue of quasibrittle materials: Sub-critical crack growth, lifetime and residual strength. *Int. J. Fatigue* **70**, 93–105 (2015).
48. H. D. Espinosa, B. C. Prorok, B. Peng, Plasticity size effects in free-standing submicron polycrystalline FCC films subjected to pure tension. *J. Mech. Phys. Solids* **52**, 667–689 (2004).
49. B. Bourdin, G. A. Francfort, J.-J. Marigo, Numerical experiments in revisited brittle fracture. *J. Mech. Phys. Solids* **48**, 797–826 (2000).
50. Z. P. Bažant, W. Luo, V. T. Chau, M. A. Bessa, Wave dispersion and basic concepts of peridynamics compared to classical nonlocal damage models. *J. Appl. Mech.* **83**, 111004 (2016).
51. J. J. C. Remmers, R. De Borst, C. V. Verhoosel, A. Needleman, The cohesive band model: A cohesive surface formulation with stress triaxiality. *Int. J. Fract.* **181**, 177–188 (2013).